

The Unsteady Growth of Ship Waves in a Towing Tank

Lawrence J. Doctors

The University of New South Wales, Sydney, NSW 2052, Australia

Email: L.Doctors@UNSW.edu.au

Summary

An extensive set of towing-tank experiments on the wave generation of three geosim catamaran models was conducted in order to test the predictive ability of *unsteady* linearized wave theory. It is demonstrated here that it is essentially impossible to achieve the steady-state wave pattern in a typical towing tank in the region of the depth-critical speed. However, the theory can be used with confidence to predict the incompletely developed wave system behind the model.

1 Introduction

Previous research on the wave generation by ships has shown that excellent agreement can be achieved between the experimental measurements and the linearized theory. The exception to this is in the neighborhood of the depth Froude number $F_d = U/\sqrt{gd}$ equal to unity, as demonstrated by Doctors (2007).

Here, we investigate the *temporal generation* of the waves, considering motion of the vessel from its start in the tank. The theory in the deep-water case for this problem was developed by Çalişal (1977).

2 Unsteady Wave Elevation

The solution to the field equation and the boundary conditions are obtained using a two-dimensional Fourier transformation from the x - y physical domain (see Figure 1(a)) to the k - θ or k_x - k_y wave-number domain. The Laplace transform is applied to the time.

The analysis is similar to that presented by Lunde (1951), leading to his Equation (16.14). In the current notation, the potential induced by a point source $Q(t)$ located at $(0, 0, z')$ is:

$$\phi = \phi_1 + \phi_2 + \phi_3, \quad (1)$$

$$\phi_1 = -\frac{Q(t)}{4\pi r} - \frac{Q(t)}{4\pi r''}, \quad (2)$$

$$\begin{aligned} \phi_2 = & \frac{Q(t)}{4\pi^2} \int_{-\pi}^{\pi} d\theta \int_0^{\infty} dk \operatorname{sech}(kd) \exp(-kd) \\ & \cdot \cosh[k(d+z)] \cosh[k(d+z')] \\ & \cdot \exp[ik(x \cos \theta + y \sin \theta)], \end{aligned} \quad (3)$$

$$\begin{aligned} \phi_3 = & -\frac{1}{4\pi^2} \int_0^t Q(\tau) d\tau \int_{-\pi}^{\pi} d\theta \int_0^{\infty} dk \\ & (gk/\omega) \operatorname{sech}^2(kd) \cdot \sin[\omega(t-\tau)] \\ & \cdot \exp\{ik[s(t) - s(\tau)] \cos \theta\} \\ & \cdot \cosh[k(d+z)] \cosh[k(d+z')] \\ & \cdot \exp[ik(x \cos \theta + y \sin \theta)]. \end{aligned} \quad (4)$$

Here, s is the distance traveled and

$$r = \sqrt{x^2 + y^2 + (z - z')^2}, \quad (5)$$

$$r'' = \sqrt{x^2 + y^2 + (z + z' + 2d)^2}, \quad (6)$$

$$\omega = \sqrt{gk \tanh(kd)}. \quad (7)$$

The wave elevation ζ can be obtained from the dynamic free-surface condition, using the potential in Equation (1). The algebra involves folding the wave-number integrals and using a multiple image-source distribution, based on thin-ship theory, in order to satisfy the tank-sidewall condition. The final result is:

$$\begin{aligned} \zeta(x, y, t) = & -\frac{i}{\pi^2} \int_0^t U(\tau) d\tau \int_0^{\infty} dk_x \sum_{i=0}^{\infty} \epsilon \Delta k_y k_x \\ & \cdot \cos[\omega(t-\tau)] \\ & \cdot \exp\{ik_x[x + s(t) - s(\tau)]\} \\ & \cdot \cos(k_y y) \cdot (\mathcal{U} - i\mathcal{V}), \end{aligned} \quad (8)$$

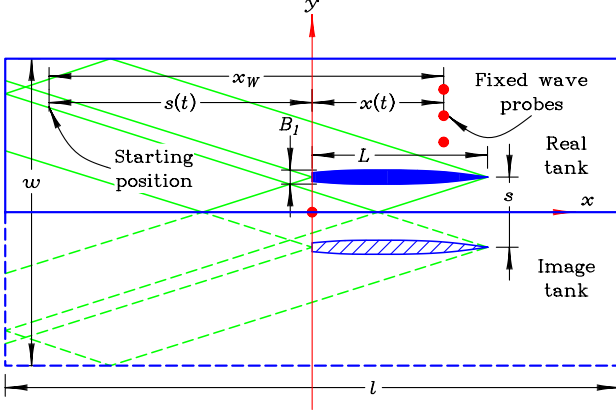


Figure 1: Definition of the Problem
(a) Experimental Setup

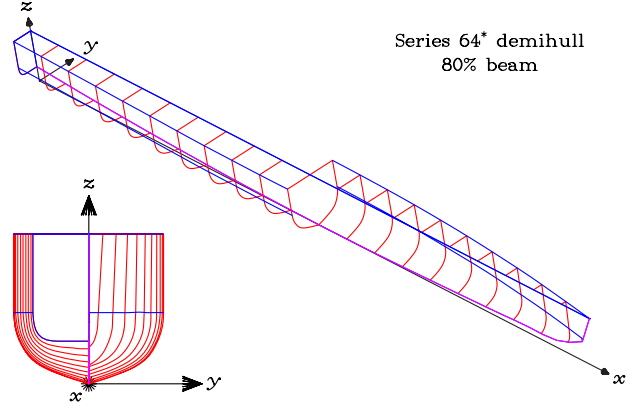


Figure 1: Definition of the Problem
(b) Demihull with 80% Beam

in which

$$k_x + ik_y = k \exp(i\theta), \quad (9)$$

$$\epsilon = \begin{cases} \frac{1}{2} & \text{for } i = 0 \\ 1 & \text{for } i \geq 1 \end{cases}, \quad (10)$$

$$k_y = i\Delta k_y, \quad (11)$$

$$\Delta k_y = 2\pi/w. \quad (12)$$

Finally, the finite-depth wave functions in Equation (8) are given by the formulas

$$\mathcal{U} = \frac{P^+ + \exp(-2kd)P^-}{1 + \exp(-2kd)}, \quad (13)$$

$$\mathcal{V} = \frac{Q^+ + \exp(-2kd)Q^-}{1 + \exp(-2kd)}, \quad (14)$$

in which the Michell (1898) deep-water functions depend on the local beam $b(x, z)$:

$$P^\pm + iQ^\pm = \int_{S_0} b(x, z) \exp(ik_x x \pm kz) \cdot \cos(k_y y) dS. \quad (15)$$

3 Steady-State Wave Elevation

The case of steady motion can be obtained from Equation (8) by setting the velocity U to be constant and taking the limit for large time. The result is:

$$\zeta(x, y) = \frac{1}{\pi^2} \int_0^\infty dk_x \sum_{i=0}^\infty \epsilon \Delta k_y k_x^2 \exp(ik_x x)$$

$$\begin{aligned} & \cdot \cos(k_y y) \cdot (\mathcal{U} - i\mathcal{V})/f \\ & - \frac{i}{\pi} \sum_{i=0}^\infty \epsilon \Delta k_y k k_x \exp(ik_x x) \\ & \cdot \cos(k_y y) \cdot (\mathcal{U} - i\mathcal{V})/\frac{df}{dk}, \end{aligned} \quad (16)$$

where the dispersion relationship and its derivative are

$$f = k^2 - k k_0 \tanh(kd) - k_y^2, \quad (17)$$

$$\frac{df}{dk} = 2k - k_0 \tanh(kd) - k k_0 d \operatorname{sech}^2(kd), \quad (18)$$

and the fundamental circular wave number is

$$k_0 = g/U^2. \quad (19)$$

4 Root-Mean-Square Wave Elevation

Figure 1(b) is a pictorial view of the thinnest test model, referred to as the 80%-beam model. This model has a transom stern. It is suitable as a high-speed vessel.

Figure 2(a) is a plot of the dimensionless root-mean-square wave elevation measured by the five wave probes, located at $y/L = 0.6667(0.3333)2.0000$, for wave cuts over the range $-7 \leq x/L \leq 0$ for the vessel with a demibeam-to-length ratio $B_1/L = 0.0742$, and a dimensionless demihull spacing $s/L =$

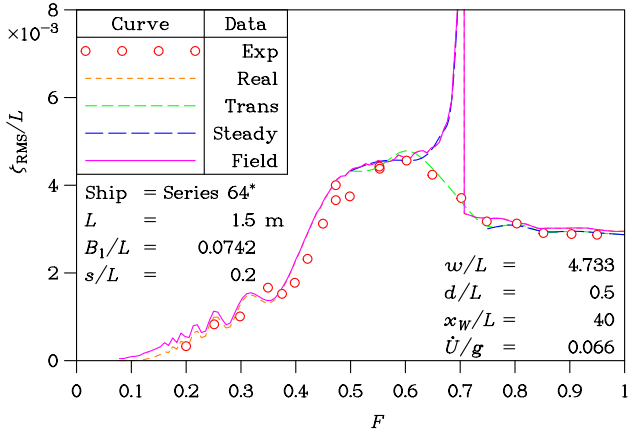


Figure 2: Steady and Unsteady Theory
(a) $B_1/L = 0.0742$ and $s/L = 0.2$

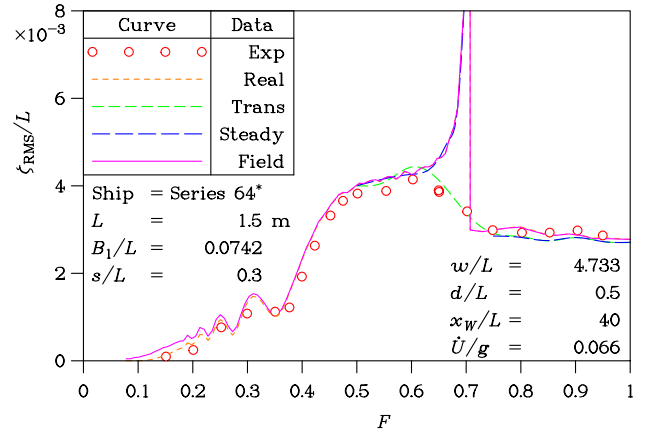


Figure 2: Steady and Unsteady Theory
(b) $B_1/L = 0.0742$ and $s/L = 0.3$

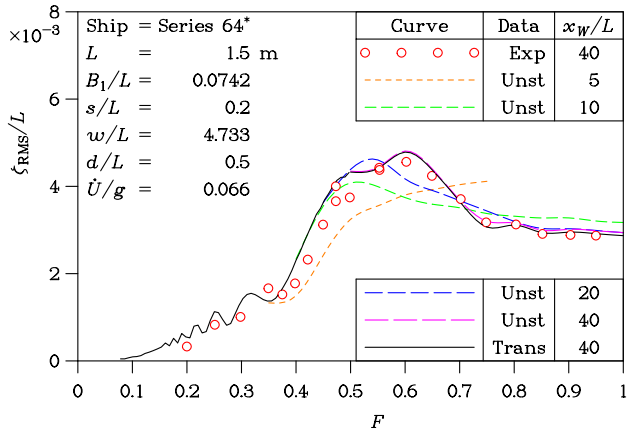


Figure 3: Location of Wave Probe
(a) $B_1/L = 0.0742$ and $s/L = 0.2$

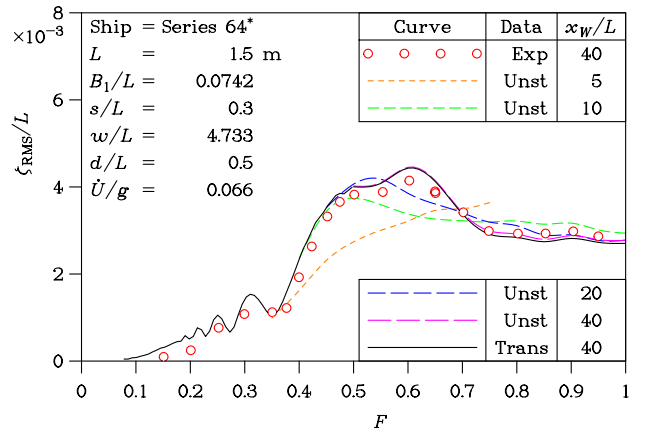


Figure 3: Location of Wave Probe
(b) $B_1/L = 0.0742$ and $s/L = 0.3$

0.2. The dimensionless carriage acceleration was $\dot{U}/g = 0.066$. Five sets of data are plotted as a function of the Froude number F . The experiments are shown as symbols and indicated as “Exp”. The first theoretical curve, referred to as “Real” is taken from Doctors (2007) and assumes typical real water properties. It is a steady-state calculation using the downstream far-field approximation and is the real-fluid equivalent of double the second term in Equation (16). One can see the generally excellent agreement, except in the troublesome region near the critical speed.

The third curve, indicated by “Trans”, is the current inviscid unsteady calculation in Equa-

tion (8), with the wave probe set at the correct experiment position $x_W/L = 40$. However, the unsteady theory has only been applied to the transverse wave whereas the traditional steady theory has been applied to all the other wave components. Excellent agreement is now achieved in the critical-speed range. The fourth curve, indicated by “Steady” is the inviscid theory from Equation (16), which very closely coincides with that indicated by “Real”, except at very low speeds. It is also almost identical to the last curve indicated by “Field”, which was computed as a downstream far-field wave system. Figure 2(b) is similar, but is for the case of a greater demi-hull spacing $s/L = 0.3$.

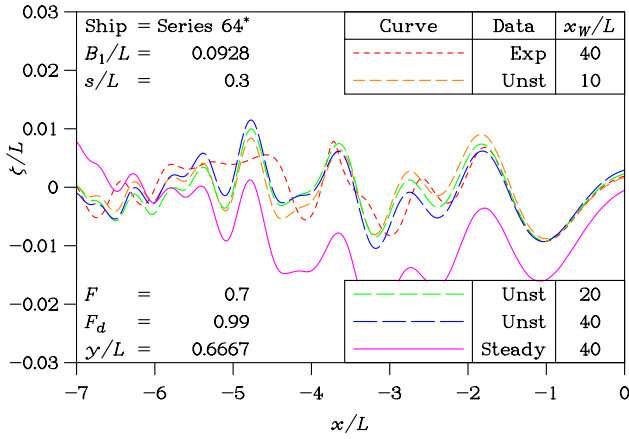


Figure 4: Growth of Wave Profile
 (a) $F = 0.7$, $F_d = 0.9899$ and $y/L = 0.6667$

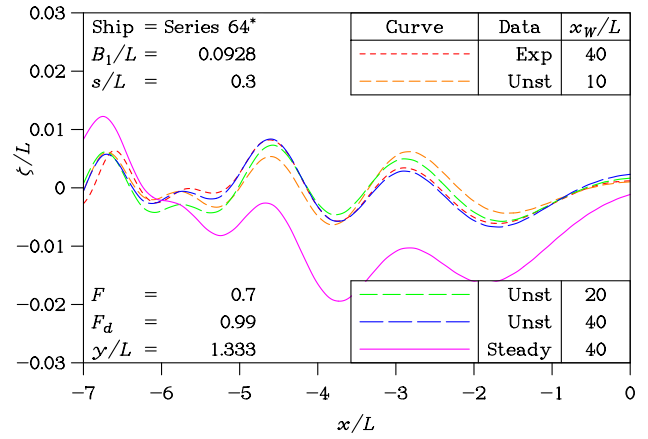


Figure 4: Growth of Wave Profile
 (b) $F = 0.7$, $F_d = 0.9899$ and $y/L = 1.3333$

Figure 3(a) corresponds to Figure 2(a). It shows the true unsteady calculations for four different assumed locations x_W/L of the wave probes. These curves are indicated as “Unst”. The general effect is that the wave magnitude increases with this parameter. The first and sixth curves have been repeated from Figure 2(a) for the purpose of comparison. Figure 3(b) applies to the greater spacing.

5 Wave-Elevation Curves

Wave profiles are presented in the two parts of Figure 4, which is for the challenging case of $F = 0.7$ or $F_d = 0.9899$. For a close wave cut $y/L = 0.6667$ in Figure 4(a), one sees the excellent agreement between the current unsteady calculation (fourth curve) and the experiments, both for $x_W/L = 40$, at least back to $x/L = -2$. The traditional steady calculation (fifth curve) is a very poor predictor. Figure 4(b), which is for the further cut $y/L = 1.333$, demonstrates excellent agreement between the unsteady prediction and the experiments for $x_W/L = 40$ over the entire length of the wave cut. Again, the steady prediction is seen to be very poor in this transcritical speed range.

6 Concluding Comments

We have demonstrated theoretically that unsteady phenomena are such as to reduce the

otherwise large theoretical wave elevations in the transcritical region. We have also shown that the unsteady effect can be traced almost entirely to the transverse wave component.

The tests were performed in the Towing Tank at the Australian Maritime College (AMC) under the supervision of Mr Richard Young and Mr Liam Honeychurch.

7 References

- ÇALIŞAL, S.: “Effect of Initial Acceleration on Ship Wave Pattern and Wake Survey Methods”, *J. Ship Research*, Vol. 21, No. 4, pp 239–247 (December 1977)
- DOCTORS, L.J.: “A Test of Linearity in the Generation of Ship Waves”, *Proc. Twenty-Second International Workshop on Water Waves and Floating Bodies (22 IWWWFB)*, Plitvice Lakes, Croatia, pp 61–64 (April 2007)
- LUNDE, J.K.: “On the Linearized Theory of Wave Resistance for Displacement Ships in Steady and Accelerated Motion”, *Trans. Society of Naval Architects and Marine Engineers*, Vol. 59, pp 25–76, Discussion: 76–85 (December 1951)
- MICHELL, J.H.: “The Wave Resistance of a Ship”, *Philosophical Magazine*, London, Series 5, Vol. 45, pp 106–123 (1898)